frontiers | Frontiers in Materials

TYPE Original Research
PUBLISHED 11 February 2025
DOI 10.3389/fmats.2025.1557889

OPEN ACCESS

EDITED BY
Jiangyu Wu,
China University of Mining and Technology, China

REVIEWED BY
Wei Zhen,
Anhui University of Science and Technology, China
Shaokang Wu,
China University of Mining and Technology, China
Zhengzheng Xie,
China University of Mining and Technology, China

*CORRESPONDENCE
Chongyan Liu,
chongyanliu@126.com

RECEIVED 09 January 2025
ACCEPTED 24 January 2025
PUBLISHED 11 February 2025

CITATION
Ma L, Liu C and Zhao G (2025) Rock fracture mode and acoustic emission characteristics under true triaxial single-sided unloading path.
Front. Mater. 12:1557889.
doi: 10.3389/fmats.2025.1557889

Rock fracture mode and acoustic emission characteristics under true triaxial single-sided unloading path

Longpei Ma[1,2], Chongyan Liu[3]* and Guangming Zhao[1,2]

[1]Key Laboratory of Safe and Effective Coal Mining Ministry of Education, Anhui University of Science and Technology, Huainan, China, [2]School of Mining Engineering, Anhui University of Science and Technology, Huainan, China, [3]Joint National-Local Engineering Research Centre for Safe and Precise Coal Mining, Anhui University of Science and Technology, Huainan, China

In underground engineering, the excavation and unloading processes of rocks are extremely complex. In-depth understanding of the fracture patterns of rocks and the characteristics of acoustic emission (AE) during this process is crucial for ensuring the safe and stable operation of underground engineering. In this study, a combination of the true triaxial disturbance unloading rock testing system and the acoustic emission system was adopted to conduct true triaxial single-sided unloading tests on several common rock types, including coal, siltstone, fine sandstone, and granite. At the same time, in order to analyze the experimental data more thoroughly, the Gaussian mixture model (GMM) clustering algorithm was introduced to perform clustering analysis on the characteristic parameters of acoustic emission, so as to explore the damage and fracture patterns of the unloading rocks. The findings indicate that as the peak strength of the rock decreases, the fractal dimension of the ultimately broken fragments becomes larger, and the cracks within the failure zone develop more comprehensively. The higher the peak strength of the rock after single-sided unloading is, the greater its axial average elastic modulus will be. The acoustic emission ringing count and the b-value curve indicate that compared with siltstone and fine sandstone, granite and coal are more prone to rock burst after unloading. In the RA-AF signals of coal and granite based on the GMM, the proportion of shear signals is as high as 66.05% and 69.21% respectively, which makes it easy to form shear cracks. While the proportions of tensile cracks in siltstone and fine sandstone are 41.43% and 56.41% respectively. Under the action of axial stress, they are prone to longitudinal splitting and form tensile cracks approximately parallel to the direction of the maximum principal stress. The research findings of this study are of great guiding significance for a deep understanding of the characteristics of different rocks during the excavation and unloading processes in underground engineering.

KEYWORDS

true triaxial unloading, single-side unloading, acoustic emission, different lithology, Gaussian mixture model

1 Introduction

With the exploitation of mineral resources and the continuous spread of tunnel construction to the deep, the deep rock mass is in a state of obvious high ground

stress under the influence of self-weight stress and tectonic stress, which leads to the occurrence of disasters such as hard rock burst or large deformation of soft rock after roadway excavation and unloading (Shi et al., 2023; Wang P. et al., 2024; Shi et al., 2024). Therefore, it is of great engineering value and scientific significance to actively explore the precursory information of mechanical properties and failure deformation of coal and rock with different lithology under single-sided unloading path, which is of great engineering value and scientific significance for forming early warning system of deep rock mass and realizing stable production of coal resources.

The true triaxial compression test is the main means to explore the mechanical properties of rock under complex stress states. The early conventional triaxial compression test usually only applied axial and lateral stresses ($\sigma1 > \sigma2 = \sigma3$) to the cylindrical sample (Li and Ma, 2024; Zhu and Chen, 2022; Sun et al., 2024), making the sample in an axisymmetric stress state, which is inconsistent with the three-dimensional unequal stress state ($\sigma1 > \sigma2 > \sigma3$) of the rock in engineering practice. In order to further understand the failure mechanism of rock unloading, a large number of scholars have carried out true triaxial unloading tests. For example, Zhao et al. (2014) studied the influence of unloading rate on rock failure characteristics through true triaxial unloading experiments. Li et al. (2018) found that under true triaxial unloading conditions, both the aspect ratio and the intermediate principal stress of the sample have an effect on the failure mode, peak strength and severity of hard rock burst. Feng et al. (2021) deeply studied the influence of intermediate principal stress σ_2 on the failure mode of specimens through true triaxial unloading test, and believed that linear Mogi criterion should be used to predict the true triaxial unloading strength of granite. Xu et al. (2019) carried out the unloading test of minimum principal stress under different initial stress and unloading rate under true triaxial compression, and analyzed the influence of initial stress and unloading rate on the bearing capacity and deformation and failure characteristics of rock. Wang et al. (2018) studied the effect of end friction effect on the failure modes of specimens in true triaxial unloading tests. Zhao et al. (2021) studied the influence of loading and unloading rates on the mechanical properties, strain energy and failure mode evolution of sandstone, and determined the crack damage stress threshold of sandstone under different loading and unloading rates.

AE is a kind of damage diagnosis technology, which evaluates the damage degree of the object by the elastic wave released when the object is broken. Since the AE technology was introduced into the stability monitoring of underground engineering in the 1950 s, for the extremely brittle materials such as rock, through the analysis and research of AE signals in the process of rock fracture, the internal changes of rock can be inferred and the failure mechanism of rock can be inverted (Liu et al., 2020; Wang C. et al., 2024; Shkuratnik et al., 2019; Liu et al., 2024). So far, AE monitoring technology has been widely used in rock mechanics tests. For example, Du et al. (2020) carried out a variety of rock mechanics tests such as Brazilian splitting, three-point bending, and uniaxial compression, and studied the AE characteristics during rock failure. He et al. (2010) used AE monitoring technology to summarize the damage process and characteristics of limestone under true triaxial single-sided unloading conditions. Yang et al. (2024) proposed a wavelet analysis method for AE signals generated by rock compression, which provides an effective method for the dynamic damage evolution of rock. Jia et al. (2017) used wavelet filtering, threshold denoising, time-frequency analysis, and other methods to analyze the secondary response characteristics of coal samples during uniaxial compression, and proposed a method for predicting coal sample failure using secondary characteristics.

Due to the significant differences in mechanical characteristics exhibited by different lithological rocks after excavation and unloading, this study selected four common rocks, including coal, siltstone, fine sandstone, and granite, during roadway excavation. The mineral composition of the four rocks was analyzed by X-Ray Diffraction (XRD). The single-sided unloading test was carried out by true triaxial disturbance unloading rock test system and AE monitoring technology. The stress-strain curves throughout the whole process from unloading to failure under loading were analyzed. Based on the ringing count, cumulative energy, b-value and peak frequency curve of AE, the failure modes of different types of rocks were distinguished. GMM was constructed to cluster the AE RA-AF signals, and the crack propagation modes were differentiated according to the clustering results. This study will contribute to a deeper understanding of the internal damage evolution laws of unloading rocks and reveal the cracking and failure characteristics of unloading surrounding rocks under different geological conditions.

2 Test method

2.1 Test equipment

The test unloading equipment adopts the TAWZ-5000/3000 Microcomputer Controlled Rock True Triaxial (Disturbance) Test System which independently developed by Anhui University of Science and Technology. As shown in Figure 1, the system mainly includes three-way independent loading and unloading device, loading and unloading control host, hydraulic control cabinet and high-pressure oil pump. It can carry out various rock mechanics tests such as cyclic loading and unloading and axial disturbance under true triaxial stress conditions. The test system can independently control the pressure in three directions in two ways of stress or displacement to carry out three-axis independent loading and unloading tests. The maximum load in the X and Y (horizontal) directions is 3,000 kN, and the maximum load in the Z (vertical) direction is 5,000 kN. The loading process is controlled by a full digital servo controller.

The AE system of test adopts Beijing soft island DS5-16 B dynamic and static AE monitoring system. The signal is collected by six AE probes. In order to minimize the interference of noise, the sampling frequency range of AE is set to 1 kHz~1 MHz, and the threshold value is 50 dB. The system can collect and locate AE events, amplitude, energy and other parameters in the process of three-dimensional positioning test in real time. These parameters can characterize the initiation and development of cracks in the process of rock failure.

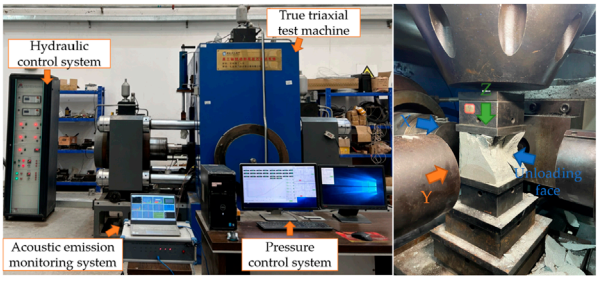

FIGURE 1
True-triaxial test system for characteristics of rock disturbance and unloading.

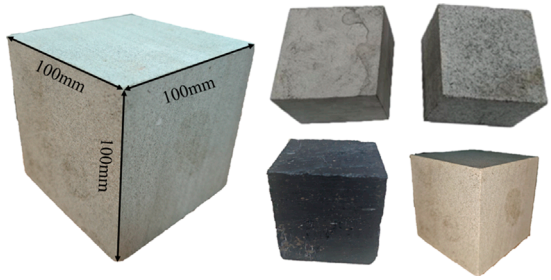

FIGURE 2
Rock specimens.

2.2 Rock specimens

In this test, four kinds of common different lithology rocks in underground engineering, such as coal, siltstone, fine sandstone and granite, were selected for single-sided unloading test. In order to reduce the influence of the discreteness of the specimen on the test results, the original rock is coring along the bedding direction, and cut and ground into a specimen with a size of 100 mm × 100 mm × 100 mm. The flatness error of the specimen surface after grinding is ±0.05, and the verticality error is ±0.30°. The processed specimen is shown in Figure 2.

Quartz has a high hardness with a Mohs hardness of 7. An increase in its content will significantly enhance the hardness and compressive strength of rocks and strengthen the ability of rocks to resist external forces. The hardness of feldspar is lower than that of quartz, with a Mohs hardness ranging from 6 to 6.5. In granite, feldspar is usually one of the mineral components with the highest content. Together with quartz, it forms the skeletal structure of the rock and enhances the compressive strength of the rock. Kaolinite is soft in texture, with a Mohs hardness generally ranging from 2 to 2.5. Due to the weak bonding force among kaolinite particles, it is prone to sliding and deformation when subjected to force, thus reducing the shear strength and compressive strength of the rock.

Since different rocks are composed of different combinations of minerals, and the content and distribution characteristics of mineral components play a decisive role in the macroscopic mechanical behaviors of rocks. Therefore, the XRD analysis technique was adopted to determine the mineral compositions and contents in the samples (Wu et al., 2024; Wu et al., 2022; Wu et al., 2020). The test results are shown in Figure 3. Coal is mainly composed of kaolinite accounting for 64.6% and muscovite accounting for 32.7%. In siltstone, quartz accounts for 71.3%, followed by kaolinite with a proportion of 15%. In fine sandstone, quartz has the highest proportion of 64.8%, followed by sodium feldspar with a proportion of 31.2%, and it also contains a small amount of kaolinite. Granite is mainly composed of quartz accounting for 48% and potassium feldspar accounting for 46%, with a small amount of other substances.

2.3 Test scheme

As shown in Figure 4, the surrounding rock of deep roadway is in the original rock stress state before excavation. After excavation, the surrounding rock forms a single-face empty unloading state. The tangential stress in the unloading area increases, and the radial stress drops to 0 (Xu et al., 2020) instantly. The cracks are compacted or developed and expanded, causing damage and cracking of the surrounding rock.

In Figure 4, σ_θ, σ_γ and σ_ν are the maximum principal stress, intermediate principal stress and minimum principal stress. The maximum principal stress σ_1 of the unloading surrounding rock unit is set to the Z-axis direction, the intermediate principal stress σ_2 is set to the Y-axis direction, and the minimum principal stress σ_3 is set to the X-axis direction.

In order to simulate the change process of surrounding rock stress after excavation of underground engineering roadway, this study adopts the test method of "true triaxial loading-single side unloading-axial loading". Before the start of the test, the sample placed in the true triaxial loading chamber is fixed with a fixture, and then the AE probe coated with Vaseline is installed at the corresponding position of the fixture. The test AE signal is synchronized with the data acquisition of the true triaxial test system. The loading in the test is controlled by force, and the stress path is shown in Figure 5.

Firstly, loads σ_1, σ_2, and σ_3 are applied simultaneously at the loading rates of 60 kN/min, 40 kN/min, and 10 kN/min respectively until they reach the predetermined values of 30 MPa, 20 MPa, and 5 MPa. Subsequently, the value of σ_2 is maintained constant to simulate the instantaneous unloading during roadway excavation. Finally, the loading rate of 60 kN/min is increased by σ_1 until the specimen fails, thereby simulating the influence of stress concentration on the surrounding rock after roadway excavation.

3 Test result analysis

3.1 Stress-strain curve analysis

The stress-strain curve is an important method to study the failure characteristics of rock (Wang G. et al., 2022; Zhang et al., 2024; Tian et al., 2023). It can completely reflect the failure process of rock from crack compaction to crack initiation, expansion and development, and then to the final formation of macroscopic fracture surface. The stress-strain curves of different lithological rocks during the test are shown in Figure 6. Taking the strain

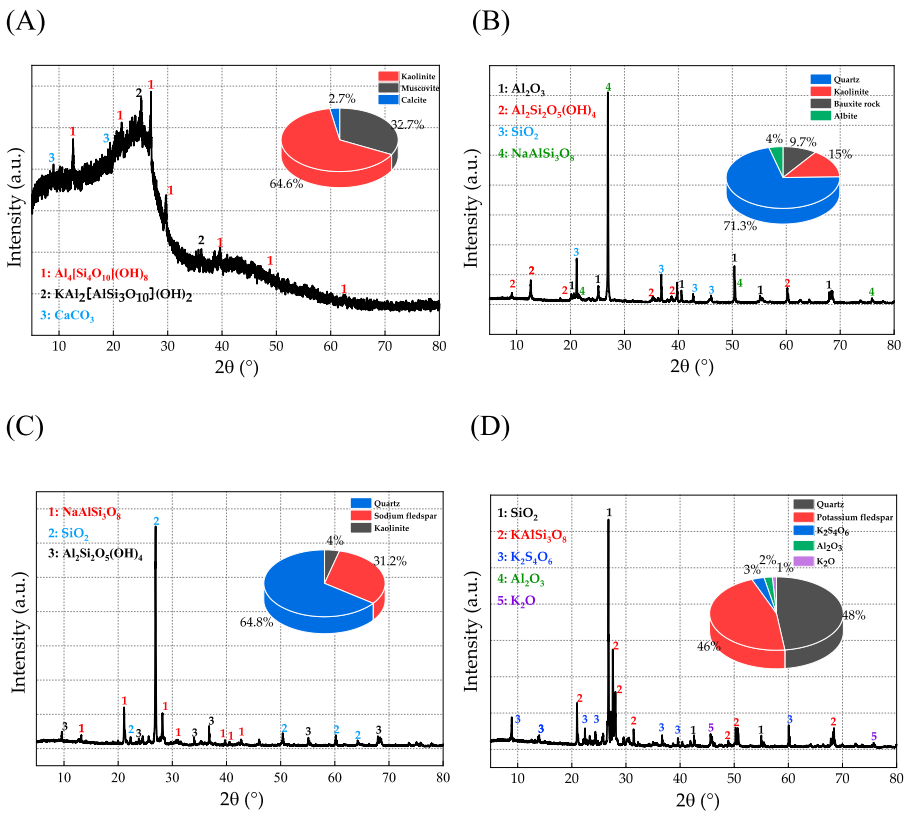

FIGURE 3
Rock XRD test: **(A)** Coal. **(B)** Siltstone. **(C)** Fine sandstone. **(D)** Granite.

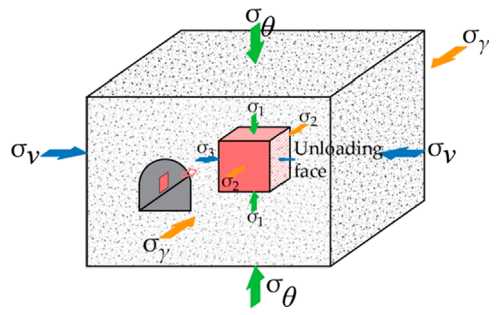

FIGURE 4
Unloading diagram.

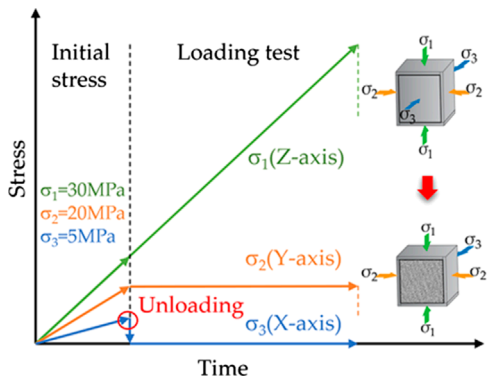

FIGURE 5
Unloading test paths for different rock properties.

of the specimen at the beginning of unloading as the reference value, the strain process of different lithologic rocks in the true triaxial unloading test is basically the same, including four stages of elasticity, crack propagation, plasticity and failure.

(1) Elasticity stage (OA): At this stage, with the increase of the maximum principal stress, the stress-strain curve of the specimen is approximately a straight line. This shows that in the triaxial compression test, the single-sided unloading of the initial stress state is not the main factor leading to rock failure. Under the condition of keeping the intermediate principal stress constant, the continuous increase of the maximum principal stress caused the failure of the specimen.

(2) Crack propagation stage (AB): With the continuous increase of the maximum principal stress, the stress-strain curve of the specimen is non-linear from point A. From the microscopic point of view, there are micro cracks in the specimen at this stage, and the volume of the specimen changes from compression to expansion.

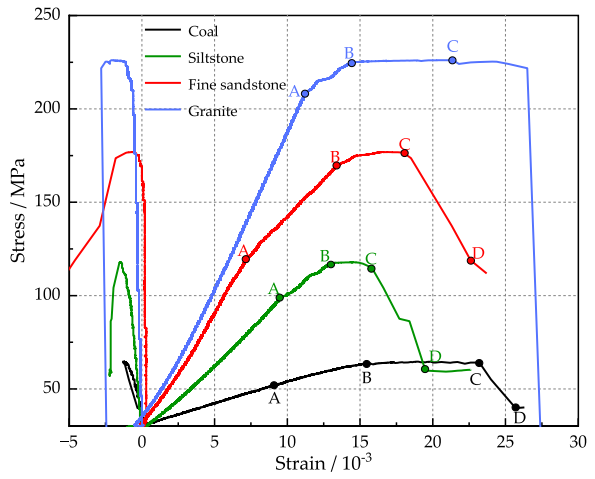

FIGURE 6
Unloading stress-strain curves for different lithologies.

(3) Plasticity stage (BC): At this stage, the crystal structure in the specimen may slip and dislocate, the relative position between the particles has also undergone irreversible adjustment, and the volume expansion rate of the specimen is accelerated. With the increase of the maximum principal stress, the small cracks and damage in the specimen expand, and the strength of the specimen decreases gradually, which leads to the gentle slope of the stress-strain curve.

(4) Failure stage (CD): At this stage, with the increase of the maximum principal stress, the cracks inside the specimen gradually penetrate and form a macroscopic fracture surface. The formation and expansion of these fracture surfaces further reduce the bearing capacity of the specimen, resulting in the stress of the specimen decreasing with the increase of strain. Due to the low stress level corresponding to the initial unloading point during the true triaxial test, the one-sided unloading in the direction of the minimum principal stress did not lead to the direct failure of the specimen, while the intermediate principal stress was kept constant, and the continuous increase of the maximum principal stress caused the failure of the specimen. This indicates that under a certain confining pressure, the friction between the broken test pieces is the main source of the residual strength of the test piece.

It can be seen from Figure 6 that with the increase of the maximum principal stress, the second principal strain shows a decreasing trend, and the expansion phenomenon occurs. The peak strength of coal, siltstone, fine sandstone and granite in the single-sided unloading test is 64.68 MPa, 117.86 MPa, 176.93 MPa and 226.12 MPa, respectively, showing an increasing trend. The peak strain of different lithologic specimens is different, but the overall change trend is similar. With the increase of the maximum principal stress, the maximum principal strain σ_1 increases continuously, while the intermediate principal strain σ_2 decreases continuously and expands laterally.

In order to evaluate the bearing capacity of different lithologic rocks after unloading, the change of unit strain force between unloading stress and 90% peak stress is counted, that is, the average elastic modulus E_A, as shown in Table 1. The harder the lithology of the rock, the higher the peak strength and the greater the average axial elastic modulus.

TABLE 1 Single-sided unloading test results.

Lithologic	Density (g/cm^3)	Peak stress (MPa)	EA (GPa)
Coal	1.37	64.68	4.85
Siltstone	2.55	117.86	11.09
Fine sandstone	2.60	176.93	12.84
Granite	2.65	226.12	17.85

3.2 Analysis of failure pattern

Under the stress state of true triaxial single-sided unloading, the expansion deformation of different lithologic specimens mainly expands along the direction of the minimum principal stress unloading surface. The failure of the specimen after single-sided unloading mainly occurs near the unloading free surface, showing obvious V-shaped failure accompanied by the spalling of rock fragments and rock particles. There is also a small V-shaped crack penetration surface near the unloading surface of the minimum principal stress, but there is no rock spalling.

As shown in Figure 7, the coal is most seriously damaged in the single-sided unloading state. Due to the large number of original fissures in the coal and the strong heterogeneity, when the coal is destroyed, the in-plane damage of the unloading free surface is the deepest, the V-shaped damage depth is deeper, the fracture surface is rough, and there are a large number of small fragments. The failure form is complex and the overall crushing is serious. The fractured rock mass in the V-shaped failure pit of siltstone is large, and the unloading surface presents tensile failure. The fine sandstone is denser and harder, and there are more shear cracks near the non-unloading surface. There are more shear cracks near the V-shaped failure pit near the unloading surface. The macroscopic tensile fracture surface is mixed with shear cracks, and there are many discontinuous cracks. The boundary between the failure shear and tensile crack surface of granite is the clearest. The spallation phenomenon of pressure-induced tensile crack in X-shaped failure pit is the most obvious, and there are many flake fragments. The failure surface in V-shaped failure pit is ladder-shaped, and the overall unstable shear crack is obvious.

Fractal geometry theory is mainly used to study nonlinear complex phenomena. It is widely used in quantitative analysis of rock damage degree (Liu C. et al., 2023; Pan et al., 2024). In order to analyze and compare the damage degree of unloading specimens with different lithology intuitively, the fractal dimension *D* of the specimen is calculated by using the relationship between the mass of the fragment and the equivalent side length to quantitatively characterize the distribution characteristics of the broken block (Zhou et al., 2023). The fractal dimension takes the fragment

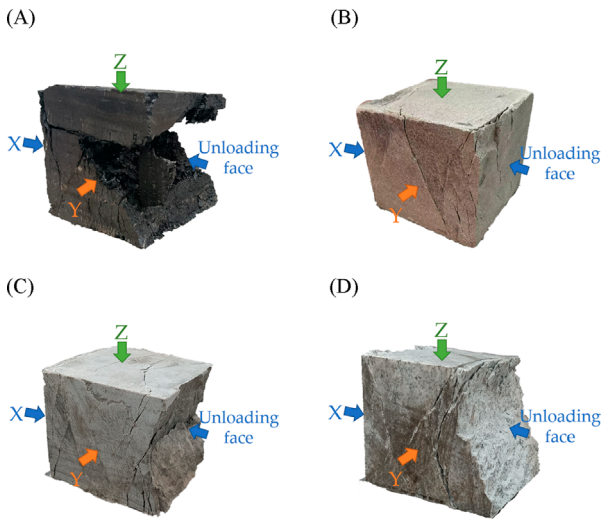

FIGURE 7
Macroscopic failure modes of unloading specimens with different lithology: **(A)** Coal. **(B)** Siltstone. **(C)** Fine sandstone. **(D)** Granite.

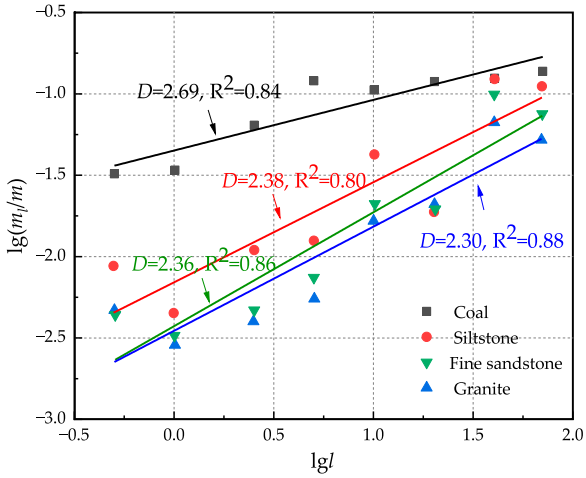

FIGURE 8
lg(m_l/*m*) and *lgl* curves of coal and rock fragments.

size of the sample as the independent variable and the mass of different grades of fragments as the dependent variable to reflect the degree of fragmentation of the test block. The greater the degree of fragmentation, the more uniform the size of the sample fragments. The fractal dimension equations of the unloading specimen are shown in Equations 1, 2 (Zhang et al., 2023):

$$D = 3 - \alpha \tag{1}$$

$$\alpha = \frac{lg(m_l/m)}{lg(m_l)} \tag{2}$$

In the formula, the independent variable α refer to is the slope value of m_l/m-l in double logarithmic coordinates, m_l is the corresponding fragment mass when the equivalent side length is l, m is the mass of the fragments in the calculated size. m_l/m is the cumulative proportion of fragments with equivalent side length less than l.

It should be noted that when calculating the fractal dimension, it is found that the self-similarity of fragments may only exist in a certain local area, which is also reflected in the research of relevant scholars (Deng et al., 2016). In order to reduce the influence of discrete points on the slope and correlation coefficient of the fitting curve of *lg*(m_l/*m*) and *lg*(m_l), the fractal dimension is calculated by selecting the specimen fragments with the fragmentation degree below 70.0 mm. According to the size characteristics of the broken specimen block, a standard sieve with a pore size of 0.5, 1.0, 2.5, 5.0, 10.0, 20.0, 40.0, and 70.0 mm was selected. The fragments of each grade of unloading specimen were weighed multiple times and averaged, and 8 groups of *lg*(m_l/*m*) and *lgl* were obtained. The linear fitting is carried out in the coordinates of *lg*(m_l/*m*) and *lgl*, and the double logarithmic relationship line about the fragmentation of the specimen is obtained. The fractal dimension D is derived from the slope of the fitted line, and R^2 is the fitting measure of the linear regression model, which measures the strength of the relationship between the fractal dimension D and the dependent variable *lg*(m_l/*m*).

The relationship between *lg*(m_l/*m*) and *lgl* of unloading rock blocks with different lithology is shown in Figure 8. The compressive strength of the unloading specimen has obvious influence on the fractal dimension of the specimen, and the fractal dimension of the unloading specimen decreases with the increase of the compressive strength of the specimen. The maximum fractal dimension of coal is 2.69, which indicates that the degree of fragmentation of coal after single-sided unloading is larger, and there are more small and medium-sized fragments. The minimum fractal dimension of granite is 2.30, the degree of fragmentation is relatively low, and the proportion of medium and high grade fragments is relatively large. The fitting measures of *lg*(m_l/*m*) and *lgl* of the four groups of unloading specimens are all greater than 0.8, showing good linearity. The degree of fragmentation of the unloading specimen is opposite to the change trend of its hardness. The smaller the peak strength of the rock, the larger the fractal dimension of the final failure debris. Correspondingly, the degree of fragmentation is higher, and crack development within the failure zone is most extensive.

3.3 Characteristics of mechanics and AE

The specimen of coal and rock mass will deform and fracture under load, and release energy in the form of elastic wave. Through the monitoring and analysis of elastic wave, the evolution process of micro behavior such as the development, expansion and penetration of micro cracks in the specimen can be obtained. At present, the research on AE signals mainly obtains the internal fracture characteristics of rocks by analyzing the characteristic parameters in the elastic wave waveform. Common parameters include ring count, amplitude, b value and peak frequency. The corresponding characteristic parameter definitions are shown in Figure 9.

The ringing count refers to the number of oscillations when the impact signal crosses the threshold value. The ringing count between unloading specimens of different lithology does not represent

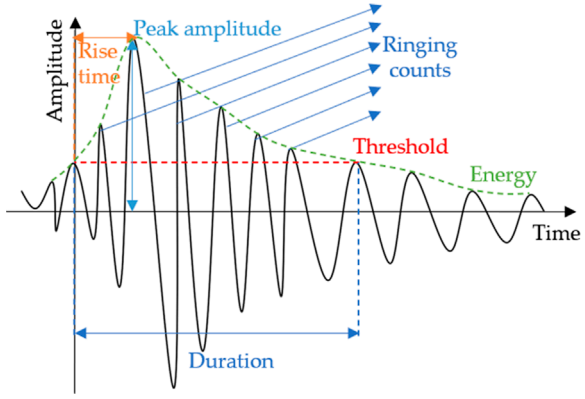

FIGURE 9
Signal and parameters of AE.

the actual damage, but it can reveal the crack propagation law of the specimen under different stress states. In order to more intuitively reflect the damage characteristics of different lithology specimens, the ringing count and cumulative energy during the test were normalized. The variation curves of AE ringing count and cumulative energy with time during the true triaxial single-sided unloading test are shown in Figure 10.

After the coal is unloaded on one side, compared with the ringing count at the time of failure, there is no obvious sudden increase in the ringing count in the 35% stress interval after unloading, indicating that the crack is developing and expanding, but there is no obvious large-scale penetration failure. The cumulative energy is nearly horizontal, and there is no obvious change, and the energy is accumulating. When the peak stress reaches 82%, the ringing count rate begins to rise gradually, and the slope of cumulative energy change gradually increases, showing an exponential trend. When the damage occurs, the ringing count rate and cumulative energy increase abruptly and reach the maximum value. This failure mode is due to the fact that most of the local fractures continue to accumulate, and the accumulated energy accumulates to a certain extent, which eventually causes the overall instability, and the continuous progressive damage in the coal body is more concentrated. The evolution law of AE signals of granite and coal is similar. For a long time after unloading, there is no obvious mutation in the ringing count rate, and the cumulative energy develops nearly horizontally. However, different from coal, in the stage of ringing count rate change, the amplitude of mutation is large, the cumulative energy increases linearly, and no damage shows the characteristics of gradual and continuous increase.

The damage of unloading specimens with siltstone and fine sandstone is more dispersed. After one-sided unloading, the AE signal shows the characteristics of intermittent occurrence, and the ringing count shows the characteristics of irregular sudden increase, accompanied by the cumulative energy jump step growth. However, before the sudden increase of most ringing count rates, the ringing count rate will continue to increase in front of the sudden increase, and gradually decrease after the sudden increase peak, and the local approximation shows a “triangle” change. It shows that the damage and failure of these two kinds of lithology is the overall instability induced by the continuous accumulation of many local fractures, and the ringing count rate does not increase continuously for a long time at the peak value, indicating that the energy accumulated in the unloading part has been gradually released. When the peak strength is unstable, it is not as severe as coal and granite. The macroscopic failure modes of different lithology specimens also show this point. Therefore, compared with siltstone and fine sandstone, granite and coal are more prone to rock burst.

3.4 Evolution characteristics of b value and peak frequency of AE

The b value is a function of the crack propagation scale and a very important parameter in the AE characteristics. Its physical meaning is the ratio of the number of AE small-magnitude events to the number of large magnitude events during the rock failure process, which can reflect the rock failure process (Qi et al., 2022). The time-varying dynamic b value can better reflect the internal crack propagation mode of the specimen at different loading stages. In order to avoid excessive error caused by too few AE events in a certain magnitude range, 1000 AE events were taken as a set of data, and 100 events were sampled and calculated by sliding, and the law of b value evolution with time was obtained.

The peak frequency of each AE signal event can be obtained by transforming the AE signal time domain signal into frequency domain signal through Fourier transform during the true triaxial single-sided unloading test of different lithologic specimens. By analyzing the changes of b value and peak frequency during the test process, the damage evolution law of different lithologic unloading specimens can be revealed. When the b value rises and the high-frequency AE signal gathers, it indicates that the specimen mainly occurs the closed development of small-scale cracks; the decrease of b value and the aggregation of low-frequency AE signals indicate that the specimen is dominated by the expansion and penetration of large-scale cracks. For the specimen with small change of b value, the internal cracks expand gradually. The significant change of b value indicates that the specimen may undergo sudden expansion. There are two reasons for the decrease of b value before rock failure and instability. One is that the micro-fracture changes from tensile fracture to shear fracture. The other is that the crack interaction is significantly enhanced.

The peak frequency-b value-time curve of unloading specimens with different lithology is shown in Figure 11. The distribution law and change trend of the main frequency distribution range of the signal in the unloading specimen during the loading process are analyzed, in which 0~90 KHz is the low frequency, 90~200 KHz is the intermediate frequency, and 200~500 KHz is the high frequency. Therefore, it provides a basis for the fracture evolution of unloading specimens with different lithology.

At the initial stage of loading, the b value of AE of coal and granite shows a small fluctuation, which reflects that the micro-fracture state changes slowly. The proportion of AE events of different sizes does not change much, and the crack state of different scales is relatively constant. With the increase of axial load, the b value of AE decreases rapidly, accompanied by the accumulation of a large number of medium and low frequency signals, indicating that the fracture mode of coal and granite changes from tensile fracture to shear fracture. In the later stage of loading, the number

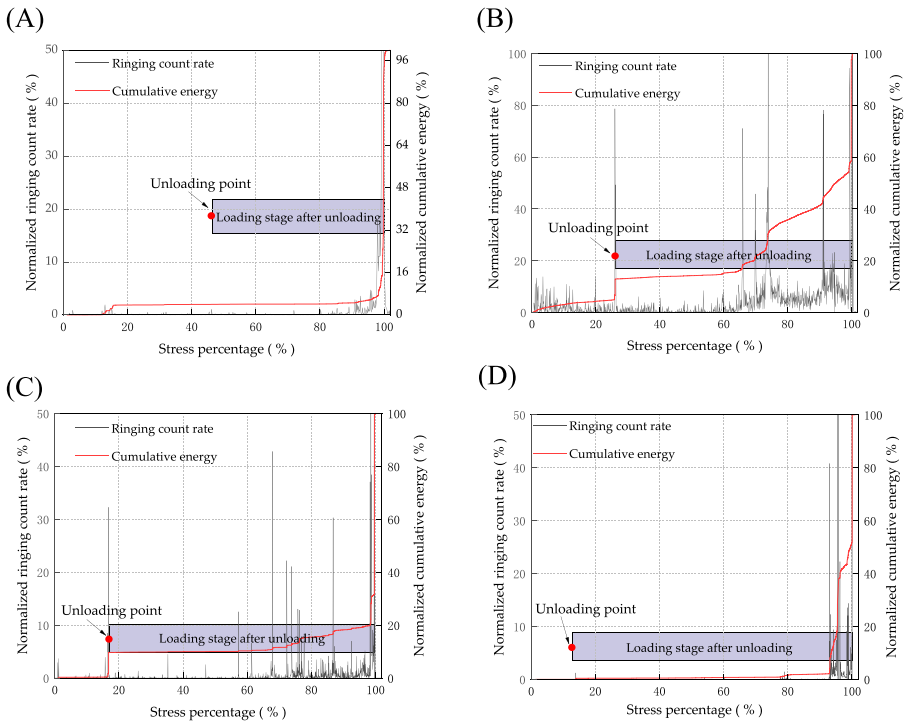

FIGURE 10
Ringing counts and energy evolution of unloading specimens of different lithologies: **(A)** Coal. **(B)** Siltstone. **(C)** Fine sandstone. **(D)** Granite.

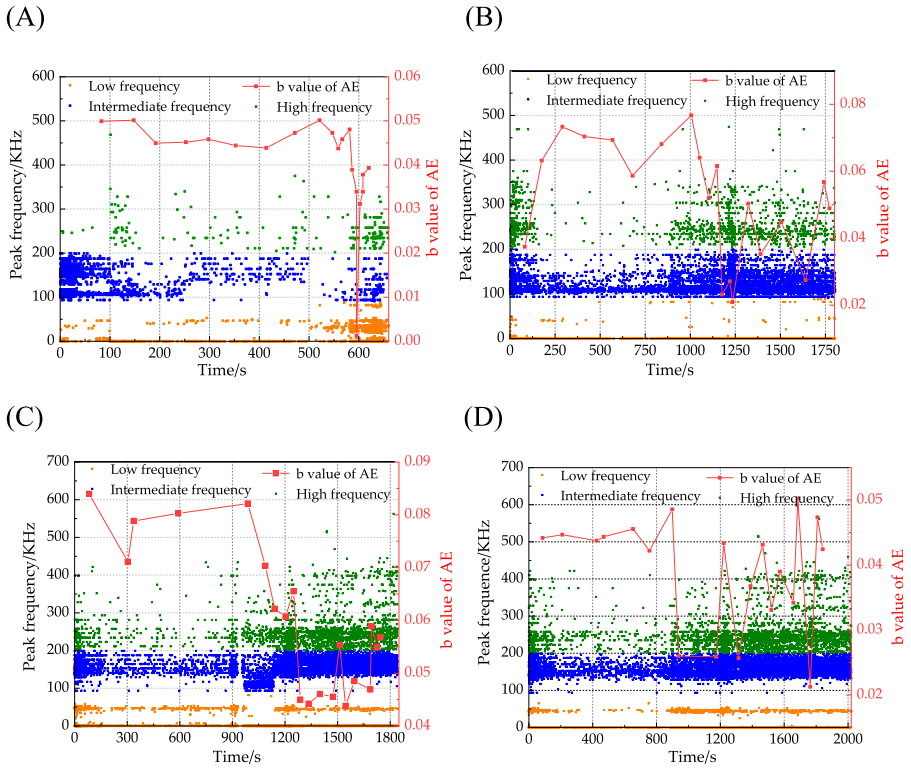

FIGURE 11
Peak frequency-b value-time curves of unloading specimens with different lithology: **(A)** Coal. **(B)** Siltstone. **(C)** Fine sandstone. **(D)** Granite.

of high-frequency and low-frequency signals of granite AE increased sharply, accompanied by b-value oscillation. This shows that at this time, the microcracks inside the granite continue to expand and connect to form macroscopic cracks, which makes the rock structure change greatly. This structural change will affect the generation and propagation of AE signals, so that the b value will oscillate.

When the coal is about to reach the bearing limit, the b value increases significantly, and the number of low, medium and high frequency signals of AE increases sharply. It shows that the coal body is relatively broken at this time, and the internal fracture surface constantly rubs and collides in the process of relative motion. With the increase of fracture surface and the intensification of motion, the degree of friction and collision increases, which leads to the increase of AE b value.

Compared with the rapid decrease of b value in the loading process of coal and granite, siltstone and fine sandstone are slightly uplifted in the process of b value decrease, which indicates that siltstone and fine sandstone are in the state of stress release at this stage. At the same time, the oscillation of b value and the aggregation of medium and high frequency signals in the later stage of loading also indicate that the damage and failure of siltstone and fine sandstone are the overall instability induced by the continuous accumulation of many local fractures. Compared with fine sandstone and siltstone, coal and granite are more prone to sudden expansion.

3.5 RA-AF characteristics

The RA and the average frequency AF in the AE characteristic parameters can characterize the type of microcracks inside the rock. RA is the ratio of the rise time to the amplitude, and AF is the ratio of the ringing count to the duration. The signal distribution characteristics of high RA and low AF represent the development and expansion of shear cracks, while high AF and low RA represent the development and expansion of tensile cracks. Predecessors have conducted in-depth research on the RA-AF characteristics of coal (Guo et al., 2021; Liu H. D. et al., 2023), and proposed to use RA-AF to characterize the crack propagation mode of coal and rock mass. As shown in Figure 12, the slope of the boundary line is defined as k. When AF/RA > k, the crack presents tensile failure, and when AF/RA < k, the crack presents shear failure.

It can be seen from Figure12 that the value of the slope k of the boundary line has a significant effect on the determination of the crack propagation mode, and the value of k does not have a clear definition standard (Dong et al., 2023; Yin et al., 2023). Therefore, in this paper, based on the GMM, combined with the maximum expectation algorithm, the model clustering results are used to distinguish the tensile cracks and shear cracks of different lithologic specimens during loading and unloading (Wang L. et al., 2022). The crack identification model based on GMM is shown in Figure 13.

Through the above model, the obtained RA-AF signal is clustered and the percentage of tensile-shear cracks is calculated. The calculation results are shown in Figure 14.

It can be seen from Figure 14 that the RA-AF signals of coal and granite under true triaxial single-sided unloading conditions are distributed in the tensile crack area and the shear crack area, but there are more signals in the shear crack area. The proportion of shear signals in the RA-AF signals of coal and granite is as high

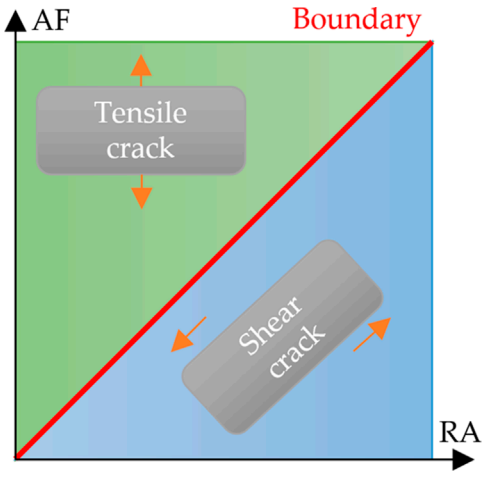

FIGURE 12
Classification standard of RA-AF signal crack types.

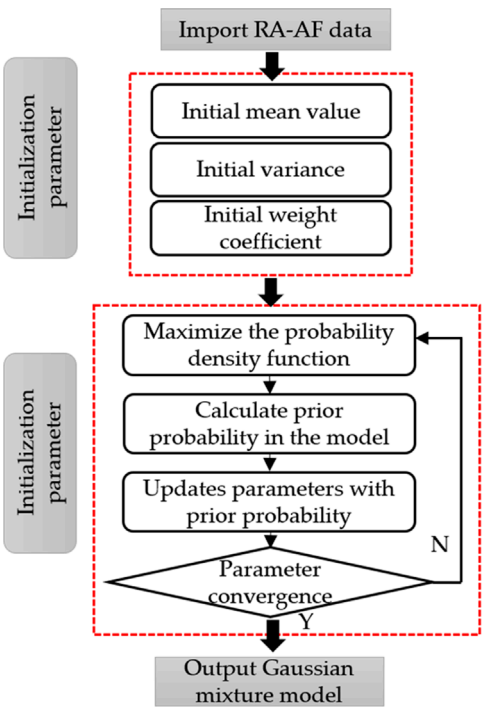

FIGURE 13
Gaussian mixture model crack identification model.

as 66.05% and 69.21%, and the macroscopic fracture mode of the unloading surface is shear failure. This shows that there are both shear cracks and tensile cracks in the process of true triaxial single-sided unloading failure of coal and granite, but shear cracks play a leading role. The internal shear stress of coal and granite first exceeds its shear strength, thus forming more shear cracks.

The proportion of tensile cracks in RA-AF signals of siltstone and fine sandstone is 41.43% and 56.41%, respectively. Compared with coal and granite, the proportion of tensile cracks in RA-AF signals of coal

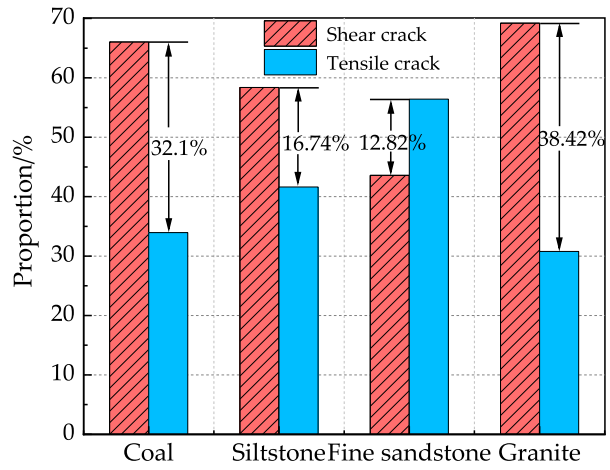

FIGURE 14
RA-AF distribution of unloading specimens with different lithology.

and granite is 33.95% and 30.79%, which is significantly increased. This shows that after single-sided unloading of sandstone, the unloading surface of sandstone is prone to longitudinal splitting under the action of axial stress, forming tensile cracks perpendicular to the direction of the maximum principal stress. It is basically consistent with the macroscopic failure mode of the unloading specimen.

4 Conclusion

This paper mainly studies the mechanical properties and AE response characteristics of rocks with different lithology under true triaxial unloading conditions. Coal, siltstone, fine sandstone and granite are selected as representative rock types. Conduct an in-depth analysis of the mineral compositions of four types of rocks with the aid of X-ray diffraction technology. The true triaxial disturbance unloading rock test system is used to carry out the true triaxial single-sided unloading test along the "vertical maximum principal stress direction loading-intermediate principal stress direction constant load-minimum principal stress direction unloading" path. On this basis, the ringing count, b value, peak frequency and RA-AF distribution characteristics of AE signals are analyzed, and the following conclusions are obtained.

(1) Under the condition of true triaxial single-sided unloading, the stress-strain curves of different lithology rocks have obvious differences, but the overall trend is similar, all of which show that with the increase of the maximum principal stress, σ_1 increases continuously, while σ_2 decreases continuously and expands laterally. The peak strength of coal is the lowest and the degree of crushing is the highest after single-sided unloading. The granite has the highest peak strength and the smallest degree of fragmentation. The peak strength of the rock is negatively correlated with the fractal dimension. The higher the peak strength, the smaller the final fractal dimension of the rock and the lower the degree of fragmentation.

(2) Before the sudden increase of the ringing count rate of siltstone and fine sandstone, the ringing count rate will continue to increase in front of the sudden increase, and gradually decrease after the sudden increase peak, and the local approximation shows a "triangle" change, indicating that the damage and failure of these two lithology is caused by the accumulation of many local fractures. There is no obvious sharp increase in the ringing count of coal and granite in the 35% stress interval after unloading. When the peak stress is 82%, the ringing count rate begins to rise gradually. This failure mode is due to the continuous accumulation of most local fractures, and the cumulative energy accumulates to a certain extent, which eventually causes the overall instability. Compared with siltstone and fine sandstone, granite and coal are more prone to rock burst.

(3) In the process of rapid decrease of b value, coal and granite are accompanied by the aggregation of low frequency signals. The siltstone and fine sandstone have a slight uplift in the process of b value decline, and the internal stress is released. Compared with fine sandstone and siltstone, coal and granite are more prone to sudden expansion.

(4) The proportion of shear signals in RA-AF signals of coal and granite is as high as 66.05% and 69.21%, and the internal shear stress is the first to exceed its shear strength, thus forming more shear cracks. The proportion of tensile cracks in siltstone and fine sandstone RA-AF signals is 41.43% and 56.41% respectively, which indicates that siltstone and fine sandstone are prone to longitudinal splitting under the action of axial stress after single-sided unloading, forming tensile cracks approximately parallel to the direction of the maximum principal stress.

Data availability statement

The original contributions presented in the study are included in the article/supplementary material, further inquiries can be directed to the corresponding author.

Author contributions

LM: Conceptualization, Methodology, Software, Writing–original draft. CL: Conceptualization, Methodology, Software, Validation, Writing–review and editing. GZ: Data curation, Validation, Writing–review and editing.

Funding

The author(s) declare that financial support was received for the research, authorship, and/or publication of this article. This study was funded by the Open Research Grant of the Joint National-Local Engineering Re-search Centre for Safe and Precise Coal Mining, China (No. EC2023026), the Scientific Research Foundation for High-level Talents of Anhui University of Science and Technology, China (No. 2023yjrc131), the National Key Research and Development Project of China (No. 2023YFC2907602), the National Natural Science Foundation of China (No. 52404068,

52004006), the National Talent Project (T2021137), the Leading Talent Project of the Special Support Plan of Anhui Province (T000508), and the Excellent scientific research and innovation team of universities in Anhui Province (2022AH010053).

Acknowledgments

The authors would like to acknowledge the discipline innovation team of Anhui University of Science and Technology.

Conflict of interest

The authors declare that the research was conducted in the absence of any commercial or financial relationships that could be construed as a potential conflict of interest.

The reviewer WZ declared a shared affiliation with the authors at the time of review.

Generative AI statement

The author(s) declare that no Generative AI was used in the creation of this manuscript.

Publisher's note

All claims expressed in this article are solely those of the authors and do not necessarily represent those of their affiliated organizations, or those of the publisher, the editors and the reviewers. Any product that may be evaluated in this article, or claim that may be made by its manufacturer, is not guaranteed or endorsed by the publisher.

References

Deng, Y., Chen, M., Jin, Y., and Zou, D. (2016). Theoretical analysis and experimental research on the energy dissipation of rock crushing based on fractal theory. *J. Nat. Gas Sci. Eng.* 33, 231–239. doi:10.1016/j.jngse.2016.05.020

Dong, L., Zhang, Y., Bi, S., Ma, J., Yan, Y., and Cao, H. (2023). Uncertainty investigation for the classification of rock micro-fracture types using acoustic emission parameters. *Int. J. Rock Mech. Min. Sci.* 162, 105292. doi:10.1016/j.ijrmms.2022.105292

Du, K., Li, X., Tao, M., and Wang, S. (2020). Experimental study on acoustic emission (AE) characteristics and crack classification during rock fracture in several basic lab tests. *Int. J. Rock Mech. Min. Sci.* 133, 104411. doi:10.1016/j.ijrmms.2020.104411

Feng, F., Chen, S., Wang, Y., Huang, W., and Han, Z. (2021). Cracking mechanism and strength criteria evaluation of granite affected by intermediate principal stresses subjected to unloading stress state. *Int. J. Rock Mech. Min. Sci.* 143 (5), 104783. doi:10.1016/j.ijrmms.2021.104783

Guo, P., Wu, S., Zhang, G., and Chu, C. (2021). Effects of thermally-induced cracks on acoustic emission characteristics of granite under tensile conditions. *Int. J. Rock Mech. Min. Sci.* 144, 104820. doi:10.1016/j.ijrmms.2021.104820

He, M. C., Miao, J. L., and Feng, J. L. (2010). Rock burst process of limestone and its acoustic emission characteristics under true-triaxial unloading conditions. *Int. J. Rock Mech. Min. Sci.* 47 (2), 286–298. doi:10.1016/j.ijrmms.2009.09.003

Jia, B., Wei, J. P., Wen, Z. H., Wang, Y. G., and Jia, L. X. (2017). The experimental research on response characteristics of coal samples under the uniaxial loading process. *Acoust. Phys.* 63, 716–722. doi:10.1134/S1063771017060057

Li, X., Feng, F., Li, D., Du, K., Ranjith, P. G., and Rostami, J. (2018). Failure characteristics of granite influenced by sample height-to-width ratios and intermediate principal stress under true-triaxial unloading conditions. *Rock Mech. and Rock Eng.* 51, 1321–1345. doi:10.1007/s00603-018-1414-4

Li, X., and Ma, Z. (2024). A novel method for imitating true-triaxial stress path with conventional triaxial apparatus. *Geomechanics and Geophys. Geo-Energy and Geo-Resources* 10 (1), 68. doi:10.1007/s40948-024-00781-x

Liu, C., Zhao, G., Xu, W., Meng, X., Liu, Z., Cheng, X., et al. (2023). Experimental study on failure characteristics of single-sided unloading rock under different intermediate principal stress conditions. *Int. J. Min. Sci. Technol.* 33 (3), 275–287. doi:10.1016/j.ijmst.2022.12.005

Liu, C. Y., Zhao, G. M., Xu, W. S., Meng, X., Huang, S. j., Zhou, J., et al. (2020). Experimental investigation on failure process and spatio-temporal evolution of rockburst in granite with a prefabricated circular hole. *J. Central South Univ.* 27 (10), 2930–2944. doi:10.1007/s11771-020-4519-3

Liu, H. D., Liu, S., Liu, H. N., Chen, J. X., Xia, Z. G., Zhai, J. Y., et al. (2023). Mechanical deterioration effect and damage evolution characteristics of soft sandstone with different water-immersed heights under uniaxial compression. *Bull. Eng. Geol. Environ.* 82 (4), 154. doi:10.1007/s10064-023-03175-7

Liu, X., Zhang, S., Xie, Y. W. T., and Wang, T. (2024). Three-dimensional heterogeneity of the pore and fracture development and acoustic emission response characteristics of coal rocks in the yunnan laochang block. *energies* 17 (5), 1207. doi:10.3390/en17051207

Pan, C., Liu, C., Zhao, G., Yuan, W., Wang, X., and Meng, X. (2024). Fractal characteristics and energy evolution analysis of rocks under true triaxial unloading conditions. *Fractal Fract.* 8 (7), 387. doi:10.3390/fractalfract8070387

Qi, M., Zhao, G., Xu, W., Cheng, X., Liu, C., Liu, Z., et al. (2022). Influence of height–diameter ratio on rock compressive failure characteristics and damage evolution law. *Energies* 15 (15), 5557. doi:10.3390/en15155557

Shi, H., Chen, W., Zhang, H., Song, L., Li, M., Wang, M., et al. (2023). Dynamic strength characteristics of fractured rock mass. *Eng. Fract. Mech.* 292, 109678. doi:10.1016/j.engfracmech.2023.109678

Shi, H., Zhang, H., Chen, W., Song, L., and Li, M. (2024). Pull-out debonding characteristics of rockbolt with prefabricated cracks in rock: a numerical study based on particle flow code. *Comput. Part. Mech.* 11 (1), 29–53. doi:10.1007/s40571-023-00607-9

Shkuratnik, V. L., Kravchenko, O. S., and Filimonov, Y. L. (2019). Stresses and temperature affecting acoustic emission and rheological characteristics of rock salt. *J. Min. Sci.* 55 (4), 531–537. doi:10.1134/S1062739119045879

Sun, B. W., Yang, S. Q., Dong, J. P., Dong, Z. J., and Tian, W. L. (2024). Experimental and GBM3D study on the failure mechanical behavior of granite with different grain sizes under conventional triaxial compression. *Bull. Eng. Geol. Environ.* 83 (11), 467. doi:10.1007/s10064-024-03964-8

Tian, Y., Weijermars, R., Zhou, F., Hu, L., Liu, T., and Liu, H. (2023). Advances in stress-strain constitutive models for rock failure: review and new dynamic constitutive failure (DCF) model using core data from the Tarim Basin (China). *Earth-Science Rev.* 243, 104473. doi:10.1016/j.earscirev.2023.104473

Wang, C., Zhang, D., Xiong, Z., Yu, B., Wang, X., Ren, F., et al. (2024). Acoustic emission noise reduction: a case of a uniaxial compression test of gypsum-like rock. *Int. J. Rock Mech. Min. Sci.* 178, 105781. doi:10.1016/j.ijrmms.2024.105781

Wang, G., Wang, R., Sun, F., and Chao, T. C. (2022). Study on characteristics of acoustic emission RA-AF and fracture modes of solution-porous limestone under uniaxial compression. *China J. Highw. Transp.* 35 (08), 118–128. doi:10.19721/j.cnki.1001-7372.2022.08.011

Wang, H., Dyskin, A., Dight, P., Pasternak, E., and Hsieh, A. (2018). Review of unloading tests of dynamic rock failure in compression. *Eng. Fract. Mech.* 225, 106289. doi:10.1016/j.engfracmech.2018.12.022

Wang, L., Li, K., Wang, Z., and Li, L. (2022). Description and prediction of stress-strain curve of loess. *Eng. Geol.* 308, 106827. doi:10.1016/j.enggeo.2022.106827

Wang, P., Zhang, N., Kan, J., Wei, Q., Xie, Z., Li, A., et al. (2024). Accumulated damage failure mechanism of anchoring structures under cyclic impact disturbance. *Int. J. Min. Sci. Technol.* 34 (12), 1693–1709. doi:10.1016/j.ijmst.2024.11.006

Wu, J., Jing, H., Gao, Y., Meng, Q., Yin, Q., and Du, Y. (2022). Effects of carbon nanotube dosage and aggregate size distribution on mechanical property and microstructure of cemented rockfill. *Cem. Concr. Compos.* 127, 104408. doi:10.1016/j.cemconcomp.2022.104408

Wu, J., Jing, H., Yin, Q., Yu, L., Meng, B., and Li, S. (2020). Strength prediction model considering material, ultrasonic and stress of cemented waste rock backfill for recycling gangue. *J. Clean. Prod.* 276, 123189. doi:10.1016/j.jclepro.2020.123189

Wu, J., Wong, H. S., Zhang, H., Yin, Q., Jing, H., and Ma, D. (2024). Improvement of cemented rockfill by premixing low-alkalinity activator and fly ash for recycling gangue and partially replacing cement. *Cem. Concr. Compos.* 145, 105345. doi:10.1016/j.cemconcomp.2023.105345

Xu, H., Feng, X. T., Yang, C., Zhang, X., Zhou, Y., and Wang, Z. (2019). Influence of initial stresses and unloading rates on the deformation and failure mechanism of Jinping marble under true triaxial compression. *Int. J. Rock Mech. Min. Sci.* 117, 90–104. doi:10.1016/j.ijrmms.2019.03.013

Xu, W., Zhao, G., Liu, C., Meng, X., Zhang, R., Kao, S., et al. (2020). Evolution mechanism of deformation and failure of surrounding rock during excavation and unloading of the high-stress rock mass. *Adv. Civ. Eng.* 2020 (1), 8863540. doi:10.1155/2020/8863540

Yang, L., Wu, B. B., Xu, Y., Fu, Y., and Xia, K. W. (2024). Damage evolution during rock dynamic compression revealed by wavelet analysis of acoustic emission signals. *Rock Mech. Rock Eng.* 57 (2), 1527–1535. doi:10.1007/s00603-023-03644-1

Yin, S., Zhou, Y., Chen, X., and Li, G. (2023). A new acoustic emission characteristic parameter can be utilized to evaluate the failure of cemented paste backfill and rock combination. *Constr. Build. Mater.* 392, 132017. doi:10.1016/j.conbuildmat.2023.132017

Zhang, Q., Lu, L. J., and Taylor, T. (2023). Remarks on the local structure of regular fractal functions with fractal dimensions. *Fractals An Interdiscip. J. complex geometry Nat.* 31 (9). doi:10.1142/S0218348X23501189

Zhang, Q., Zuo, S., Wu, D., and Yuan, X. (2024). Strain softening characteristics and stress–strain relationship of Guiyang carbonate laterite. *Bull. Eng. Geol. Environ.* 83 (4), 121. doi:10.1007/s10064-024-03615-y

Zhao, H., Song, Z., Zhang, D., Liu, C., and Yu, B. (2021). True triaxial experimental study on mechanical characteristics and energy evolution of sandstone under various loading and unloading rates. *Geomechanics Geophys. Geo-Energy Geo-Resources* 7 (1), 22–17. doi:10.1007/s40948-020-00212-7

Zhao, X. G., Wang, J., Cai, M., Cheng, C., Ma, L. K., Su, R., et al. (2014). Influence of unloading rate on the strainburst characteristics of beishan granite under true-triaxial unloading conditions. *Rock Mech. and Rock Eng.* 47 (2), 467–483. doi:10.1007/s00603-013-0443-2

Zhou, Z., Zhao, C., and Huang, Y. (2023). Nonlinear time series analysis of limestone rock failure process. *Measurement* 206, 112259. doi:10.1016/j.measurement.2022.112259

Zhu, B., and Chen, Z. (2022). Calibrating and validating a soil constitutive model through conventional triaxial tests: an in-depth study on CSUH model. *Acta Geotech.* 17 (8), 3407–3420. doi:10.1007/s11440-021-01432-1